COMMUNICATION

Check for updates

Morpholine-modified permethyl β-cyclodextrin supramolecular nanoparticles for precise dual-targeted imaging†

Jie Niu, Yao-Hua Liu, Wenshi Xu, Wen-Wen Xu, Ya-Hui Song, Jie Yu, Ying-Ming Zhang* and Yu Liu [iD] *

Possessing dual-targeted agents toward the lysosome and cancer cells, a ternary supramolecular assembly was constructed by a morpholine-modified permethyl β-cyclodextrin, sulfonated porphyrin, and folic acid-modified chitosan *via* multivalent interactions. As compared with free porphyrin, the obtained ternary supramolecular assembly showed promoted photodynamic effect and achieved dual-targeted precise imaging in cancer cells.

Macrocycle-derived supramolecular theranostics that combine two or more modalities of diagnosis and therapy in a hierarchically self-assembling manner have been proven as a novel and powerful strategy in the battle against many life-threatening diseases.[1] There are some inherent advantages of such multicomponent nanosystems. First, drug molecules and diagnostic agents with appropriate molecular size can be encapsulated in the cavity of the macrocycles through host–guest complexation. For instance, many π-aromatic chromophores stay at a silent state with poor photostability and low quantum yield but become more effective photosensitizers when they are included by a certain macrocyclic receptor, such as cyclodextrin and cucurbituril.[2] Moreover, secondary supramolecular assembling processes can be further achieved with the assistance of multivalent intermolecular noncovalent interactions.[3] In this context, polymeric,[4] amphiphilic species[5] and multicomponent assemblies[6] are considered as the most appealing candidates because numerous anchoring points exist on these molecular skeletons. Therefore, many efforts have been devoted to the fabrication of biocompatible hierarchical supramolecular nanoassemblies, which can not only induce distinct morphological changes and intriguing physicochemical properties, but also bring about fascinating theranostic modalities and outcomes, such as

multicolor subcellular/tissue imaging,[7] cancer cell apoptosis,[8] and tumor ablation.[9]

More systematic studies have demonstrated that the introduction of targeting ligands is an operationally simple and convenient approach to endow the supramolecular theranostic nanosystems with desired affinity and selectivity toward the intended sites of action in a disease model. Diverse targeting ligands have been developed in the construction of bioactive supramolecular nanoplatforms at different molecular scales, such as small organic molecules,[10] medium molecular weight polypeptides,[11] and high molecular weight polymers.[12] In this regard, along with the rapid development of targeted supramolecular nanoassemblies, there is a growing consensus that synergistic therapeutic outcomes can be readily achieved by combined usage of several targeting agents together.[13] Superior to the single-target systems, the multi-pronged approach can largely ensure precision treatments and meet customizable demands.

With a clear understanding of the superiorities of multi-targeted supramolecular assemblies and their potential in disease theranostics, we herein report a ternary nanoparticulate assembly *via* a two-step noncovalent modification process, with two different targeted ligands in a single molecular entity for efficient subcellular imaging and cancer cell death. Taking advantage of the extremely strong host–guest complexation between the morpholine-modified permethyl β-cyclodextrin (MPCD) and the sulfonated porphyrin (TPPS) up to 10^{11} M^{-2} order of magnitude in water, the formed complex in a 2:1 binding stoichiometry can not only enhance the fluorescence emission intensity of the porphyrin core by inhibiting π-stacking, but also endow the binary complex with the desired targeting ability toward lysosomes. Further assembling with folic acid-modified quaternary ammonium salt chitosan (FACA) can lead to the formation of supramolecular nanoparticles and display high accumulation in the lysosomes of cancer cells and efficient generation of reactive oxygen species to induce more pronounced cell death under light irradiation. Consequently,

*College of Chemistry, State Key Laboratory of Elemento-Organic Chemistry, Nankai University, Tianjin 300071, P. R. China. E-mail: ymzhang@nankai.edu.cn,
yuliu@nankai.edu.cn*
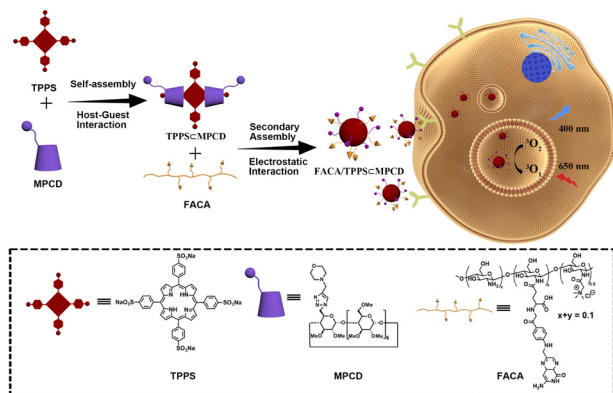
Scheme 1 Schematic illustration of ternary dual-targeted supramolecular assembly FACA/TPPS⊂MPCD.

the TPPS can be readily internalized in cells and the photophysical behaviors of the obtained ternary supramolecular self-assembly can be dramatically enhanced, thus showing better positioning capability in lysosomes and more significant photodynamic effect toward cancer cells (Scheme 1).

The morpholine-modified permethyl β-cyclodextrin (MPCD) was obtained by a 'click' reaction between azide-containing permethyl β-cyclodextrin (N₃-PCD) and 4-propargylmorpholine (Fig. S2–S4, ESI†). Meanwhile, folic acid-grafted quaternary ammonium chitosan (FACA) was synthesized *via* amide condensation (Fig. S5 and S6, ESI†).[14]

First, ^1H NMR spectroscopy was employed to examine the host–guest binding behaviors between MPCD and TPPS. As shown in Fig. S7 (ESI†), the H_{c-d} protons of TPPS exhibited a downfield shift after the addition of MPCD, and the H_{a-b} protons were split into two sets of groups. Moreover, the proton of the triazole ring also shifted downfield, which might result from the formed hydrogen bond between the triazole and the sulfonate of the TPPS. Also, 2D NOESY spectroscopy showed strong NOE correlation signals between MPCD and TPPS (Fig. S8, ESI†). These phenomena indicate the formation of a host–guest complex between MPCD and TPPS. To further investigate their binding behavior, Job's plot was determined by using UV-Vis spectroscopy (Fig. S9a, ESI†), from which the 1:2 binding stoichiometry between TPPS and MPCD was clearly determined. UV-Vis titration was carried out to calculate their binding constants (Fig. S9b, ESI†), and the absorption intensity gradually increased upon addition of MPCD (Fig. S10, ESI†). Through the non-linear curve fitting, the binding constants (K) were determined to be $K_1 = 9.95 \times 10^4$ M^{-1} and $K_2 = 5.24 \times 10^5$ M^{-1}.

Subsequently, the photoluminescence properties of TPPS were explored before and after complexation with MPCD. As shown in Fig. S11 (ESI†), under 410 nm excitation, the fluorescence intensity increased at 646 nm and 713 nm in the presence of MPCD. The existing π-stacking in TPPS could seriously affect its photophysical behaviors. Conversely, benefitting from the strong inclusion complexation with the bulky MPCD, the undesired aggregation-caused quenching was largely inhibited and the emissive path of TPPS revived to remarkably augment the fluorescence efficiency in the presence of MPCD. Due to the

acidic environment in cancer cells, the photophysical properties of MPCD and TPPS were studied under acidic conditions, which gave very similar results to that at pH 7.2 (Fig. S12 and S13, ESI†). Apparently, such inclusion-enhanced emission would greatly facilitate the cell-imaging and photosensitizing performance in the biological environment, as discussed below.

Although the morpholine motif in the TPPS⊂MPCD complex was used to target lysosomes at the subcellular level, it could not distinguish the malignant cells from the normal ones. Therefore, folic acid-grafted chitosan (FACA) was introduced to endow the binary TPPS⊂MPCD complex with the desired cell-targeting ability through multiple electrostatic interactions, due to the overexpressed folate receptors on the surface of cancer cells.

Next, TEM spectroscopy was employed to investigate the intuitive morphology of the obtained ternary self-assembly. As discerned from Fig. S14 (ESI†), no regular morphology could be observed in the free FACA or TPPS⊂MPCD complex. In contrast, the nanoparticles with a diameter of *ca.* about 500 nm could be observed upon addition of FACA with TPPS⊂MPCD complex (Fig. 1a), indicating that the multiple electrostatic attractions play an indispensable role in the formation of nanoparticulate supramolecular assemblies. The optimal concentration between FACA and TPPS⊂MPCD complex was studied and obtained as 1 mg/ml FACA with 1 mM TPPS and 2 mM MPCD (Fig. S15, ESI†). Along with the morphological information in the solid state, the hydrated diameter of the ternary nanoparticles was determined to be 524 nm from the dynamic light scattering (DLS) results (Fig. 1b). Accordingly, the Tyndall effect of the FACA/TPPS⊂MPCD assembly was more obvious than that of FACA and the TPPS⊂MPCD complex, once again indicative of the formation of large-sized aggregates in aqueous solution (Fig. S16, ESI†). In addition, the surface charge distribution was also investigated, showing that the zeta potential of the TPPS⊂MPCD complex was changed from −39.71 to 5.50 mV in the presence of FACA (Fig. 1c). This result further corroborates that the positively charged FACA was distributed and wrapped onto the outer layer of the nanoparticles, which could facilitate the close contact of FA with its receptor and eventual internalization in cancer cells.

Next, the photophysical and photochemical properties of the FACA/TPPS⊂MPCD assemblies were investigated. As can be seen from the UV-Vis spectra, the absorption intensity was sharply reduced upon addition of FACA with TPPS solution, which is probably originated from the electrostatic attraction
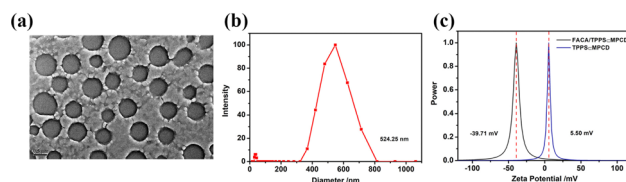

Fig. 1 (a) TEM image, (b) DLS result of the FACA/TPPS⊂MPCD assembly and (c) zeta potentials of the TPPS⊂MPCD complex and FACA/TPPS⊂MPCD assembly.

between TPPS and CA in the ternary assembly (Fig. S17a, ESI†). Meanwhile, the fluorescence intensity of pristine TPPS was also reduced in the presence of FACA (Fig. S17c, ESI†). In contrast, no obvious spectroscopic change was found when FACA was added to the solution of TPPS⊂MPCD complex, mainly due to the strong host–guest complexation, which could efficiently prevent the TPPS core from close communication with FACA (Fig. S17b and d, ESI†). The NMR data supported that the addition of FACA to the TPPS⊂MPCD complex would not influence the host–guest complexation (Fig. S18 and S19, ESI†). These results also indicate that the introduction of polymeric FACA could not have any negative impact on the photophysical performance of the included porphyrin. Moreover, 9,10-anthra-cenediyl-bis(methylene) dimalonic acid (ABDA) was employed to investigate the efficiency in the reactive oxygen species (ROS) generation, including singlet oxygen ($^1O_2$). As presented in Fig. 2a, 20.3% of ABDA was decomposed with free TPPS under light irradiation (>420 nm) for 15 min. The TPPS⊂MPCD complex at a molar ratio of 1 : 2 showed a relatively faster rate of decomposition and 25.9% of ABDA was decomposed under the same conditions. In comparison, the FACA/TPPS⊂MPCD assembly exhibited the best ROS generation ability and 35.2% of ABDA was decomposed under white light irradiation. The ROS generation of the TPPS⊂MPCD complex in an acidic environment showed no significant difference compared with that in neutral solution (Fig. S20, ESI†). These results jointly demonstrate that the successive noncovalent decoration of TPPS with MPCD and CA shells could provide a more biocompatible microenvironment to largely improve the photophysical activities of TPPS, thus making it a good candidate for dual-targeted precise imaging in cancer cells.

Furthermore, laser scanning confocal microscopy (LSCM) and flow cytometry were employed to explore the subcellular distribution of the obtained ternary assembly in the cellular environment. The fluorescence emission in HeLa cells was ana-lyzed by flow cytometry after incubation with TPPS, TPPS⊂MPCD complex, and FACA/TPPS⊂MPCD assembly for 24 h, respectively. Among all the examined groups, the strongest fluorescence

intensity was detected in the FACA/TPPS⊂MPCD assembly, sug-gesting the highest uptake efficiency with the assistance of MPCD and FACA (Fig. 2b). Accordingly, the LSCM images also gave the brightest red fluorescence emission in the FACA/TPPS⊂MPCD group (Fig. 2c). For TPPS alone possessing intense negative charges, it is indeed difficult to enter the cells. In addition, only slight red fluorescence could be observed in the TPPS⊂MPCD complex group. Apparently, benefitting from the targeting ability of FA motifs, the ternary FACA/TPPS⊂MPCD assembly could efficiently internalize in the cancer cells. Moreover, the colocaliza-tion experiments were also performed to verify the preferential accumulation at the subcellular level. As expected, the red fluores-cence of TPPS in the FACA/TPPS⊂MPCD assembly perfectly overlapped with the commercial fluorescence dye LysoTracker Green, and the Pearson correlation coefficient was 0.64 (Fig. S21, ESI†) thus confirming the precise positioning of ternary assembly in lysosomes. To verify the lysosome targeting ability, the cell imaging property was examined without the morpholine motif. As shown in Fig. S22 (ESI†), the FACA/TPPS⊂PCD assembly showed poor overlap with LysoTracker Green and the Pearson correlation coefficient was only 0.34 (Fig. S23, ESI†).

To test the cytotoxicity of the FACA/TPPS⊂MPCD assembly, the intracellular ROS levels were investigated using the com-mercially available probe 6-carboxy-2′,7′-dichlorodihydro-fluorescein diacetate (DCFH-DA) under light irradiation. As discerned from Fig. 3a, the HeLa cells treated with TPPS and TPPS⊂MPCD complex showed an inappreciable green fluores-cence signal, whereas the FACA/TPPS⊂MPCD group gave the brightest green fluorescence, corresponding to the highest ROS level upon light irradiation. These results were also consistent with the flow cytometry experiments, in which the highest uptake efficiency was given in the FACA/TPPS⊂MPCD assem-bly. Next, cell counting kit-8 (CCK8) assays were conducted to investigate the targeted anticancer ability of this ternary sys-tem. The HeLa cancer cells were incubated in the dark for 24 h and the cell viability was detected. As presented in Fig. 3b, more
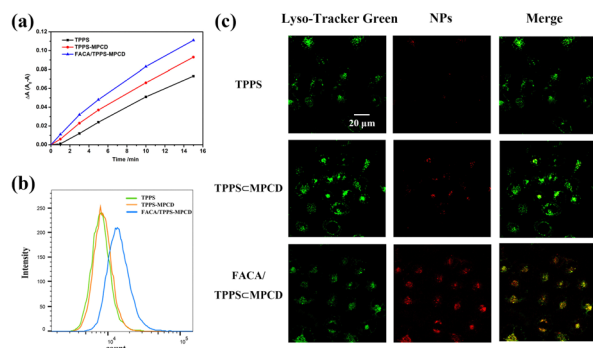

Fig. 2 (a) Decomposition rates of ABDA at 378 nm *versus* different irradiation times. (b) Flow cytometric analysis of HeLa cells in the panel and (c) lysosome colocalization CLSM images in living HeLa cancer cells treated with TPPS, TPPS⊂MPCD complex, and FACA/TPPS⊂MPCD assembly, respectively.
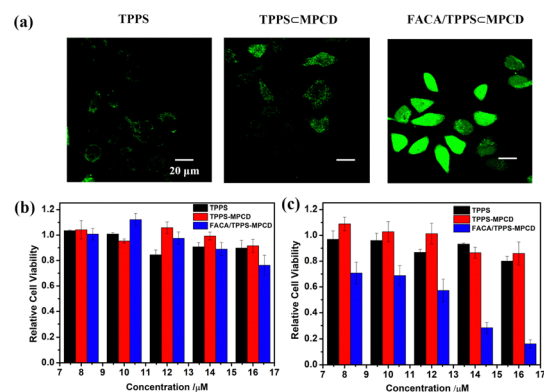

Fig. 3 (a) Intracellular $^1O_2$(ROS) detection in HeLa cells treated with TPPS, TPPS⊂MPCD complex, and FACA/TPPS⊂MPCD assembly, respectively ([TPPS] = 10 μM). *In vitro* cell viability of HeLa cells (b) in the dark and (c) under light irradiation with TPPS, TPPS⊂MPCD complex, and FACA/TPPS⊂MPCD assembly, respectively. The concentrations were calculated based on TPPS.

than 80% of cells remained alive, indicating that no dark toxicity was observed without light irradiation. However, after being irradiated under white light (>420 nm) for 10 min, the cell viability in the FACA/TPPS⊂MPCD group decreased sharply as the concentration increased (Fig. 3c). The half-maximal inhibitory concentration (IC_{50}) of the FACA/TPPS⊂MPCD assembly was 12.2 μM. Taking the concentration of TPPS at 16 μM as an example, more than 80% of cells were dead upon exposure to light irradiation. Comparatively, the cell viability was still maintained at 80% in the groups of TPPS and the TPPS⊂MPCD complex under the same conditions. These results largely contributed to the dual targeting abilities of FACA and MPCD that could remarkably improve the uptake efficiency of TPPS and the location in the lysosomes of cancer cells. In the control experiments, MRC-5 cells were employed to investigate the side effects of the resultant ternary system on the normal cells. More than 78% of cells could be detected alive at a concentration of 16 μM, indicating that this ternary system could remarkably enhance the anticancer activities towards cancer cells but reduce its side effects on normal cells (Fig. S24, ESI†).

In summary, lysosome-targeted cyclodextrin derivative MPCD was successfully synthesized and could form a strong host–guest complex with TPPS. The inclusion complexation could largely reduce the π-stacking among pristine TPPS and then endow the resultant assembly with enhanced fluorescence emission intensity and ROS efficiency. Meanwhile, the binary host–guest complex could be conveniently converted to ternary supramolecular nanoparticles by coating with polymeric FACA *via* multiple electrostatic interactions. Flow cytometry and laser confocal scanning microscopy results have proven the higher uptake efficiency of TPPS into the cancer cells and excellent colocation ability in the lysosomes, due to the dual targeting ability both at the subcellular and cellular levels. More remarkably, the obtained ternary system could induce more obvious cell death toward cancer cells, but has negligible side effects on the normal cells. It can be envisioned that the hierarchically multi-pronged assembling method can provide a convenient route for the fabrication of multiple targeting nanosystems and may expand the potential applications of supramolecular chemistry in the biomedical fields.

Conflicts of interest

There are no conflicts to declare.

Notes and references

1 (a) J. Zhou, L. Rao, G. Yu, T. R. Cook, X. Chen and F. Huang, *Chem. Soc. Rev.*, 2021, **50**, 2839; (b) Y. Cao, X.-Y. Hu, Y. Li, X. Zou, S. Xiong, C. Lin, Y.-Z. Shen and L. Wang, *J. Am. Chem. Soc.*, 2014, **136**, 10762; (c) M. Hao, G. Sun, M. Zuo, Z. Xu, Y. Chen, X.-Y. Hu and L. Wang, *Angew. Chem., Int. Ed.*, 2020, **59**, 10095.

2 (a) M. Tang, Y. Song, Y.-L. Lu, Y.-M. Zhang, Z. Yu, X. Xu and Y. Liu, *J. Med. Chem.*, 2022, **65**, 6764; (b) K. Kano, R. Nishiyabu, T. Asada and Y. Kuroda, *J. Am. Chem. Soc.*, 2002, **124**, 9937; (c) I. M. Mavridis and K. Yannakopoulou, *J. Med. Chem.*, 2020, **63**, 3391; (d) X.-D. Xu, L. Zhao, Q. Qu, J.-G. Wang, H. Shi and Y. Zhao, *ACS Appl. Mater. Interfaces*, 2015, **7**, 17371; (e) W.-L. Zhou, W. Lin, Y. Chen and Y. Liu, *Chem. Sci.*, 2022, **13**, 7976; (f) J. Chen, Y. Zhang, Y. Zhang, L. Zhao, L. Chen, Y. Chai, Z. Meng, X. Jia, Q. Meng and C. Li, *Chin. Chem. Lett.*, 2021, **32**, 3034.

3 (a) X. Dai, X. Dong, Z. Liu, G. Liu and Y. Liu, *Biomacromolecules*, 2020, **21**, 5369; (b) J. Zhou, G. Yu, J. Yang, B. Shi, B. Ye, M. Wang, F. Huang and P. J. Stang, *Chem. Mater.*, 2020, **32**, 4564; (c) X. Wu, Y. Chen, Q. Yu, F.-Q. Li and Y. Liu, *Chem. Commun.*, 2019, **55** 4343.

4 K. Yang, G. Yu, Z. Yang, L. Yue, X. Zhang, C. Sun, J. Wei, L. Rao, X. Chen and R. Wang, *Angew. Chem., Int. Ed.*, 2021, **60**, 17570.

5 (a) X.-Y. Hu, Z.-Y. Hu, J.-H. Tian, L. Shi, F. Ding, H.-B. Li and D.-S. Guo, *Chem. Commun.*, 2022, **58**, 13198; (b) H. Lu, Y. Zhao, S. Qin, Y. Zhang, J. Liu, J. Zhang, C. Feng and W. Zhao, *Adv. Fiber Mater.*, 2023, **5**, 377.

6 (a) Z. Liu, X. Dai, Y. Sun and Y. Liu, *Aggregate*, 2020, **1**, 31; (b) Z. Liu and Y. Liu, *Chem. Soc. Rev.*, 2022, **51**, 4786.

7 (a) H.-J. Yu, Q. Zhou, X. Dai, F.-F. Shen, Y.-M. Zhang, X. Xu and Y. Liu, *J. Am. Chem. Soc.*, 2021, **143**, 13887; (b) S. H. Alamudi, R. Satapathy, J. Kim, D. Su, H. Ren, R. Das, L. Hu, E. Alvarado-Martínez, J. Y. Lee, C. Hoppmann, E. Peña-Cabrera, H.-H. Ha, H.-S. Park, L. Wang and Y.-T. Chang, *Nat. Commun.*, 2016, **7**, 11964; (c) D. I. Danylchuk, P.-H. Jouard and A. S. Klymchenko, *J. Am. Chem. Soc.*, 2021, **143**, 912; (d) X.-K. Ma, X. Zhou, J. Wu, F.-F. Shen and Y. Liu, *Adv. Sci.*, 2022, **9**, 2201182; (e) N. Mehwish, X. Dou, Y. Zhao and C.-L. Feng, *Mater. Horiz.*, 2019, **6**, 14.

8 (a) Z.-Q. Li, Y.-M. Zhang, H.-Z. Chen, J. Zhao and Y. Liu, *J. Org. Chem.*, 2013, **78**, 5110; (b) S. Ziyan, M. Ning, W. Feng, R. Jiaming, H. Chenxi, C. Shuang, P. Yuxin and P. Zhichao, *Chin. Chem. Lett.*, 2022, **33**, 4563.

9 (a) Q. Zhang, M. He, X. Zhang, H. Yu, J. Liu, Y. Guo, J. Zhang, X. Ren, H. Wang and Y. Zhao, *Adv. Funct. Mater.*, 2022, **32**, 2112251; (b) Q. Yu, Y.-M. Zhang, Y.-H. Liu, X. Xu and Y. Liu, *Sci. Adv.*, 2018, **4**, eaat2297.

10 (a) X. Dai, M. Huo, B. Zhang, Z. Liu and Y. Liu, *Biomacromolecules*, 2022, **23**, 3549; (b) C. Chen, J. Ke, X. E. Zhou, W. Yi, J. S. Brunzelle, J. Li, E.-L. Yong, H. E. Xu and K. Melcher, *Nature*, 2013, **500**, 486.

11 (a) M. Tang, Y.-H. Liu, H. Liu, Q. Mao, Q. Yu, H. Kitagishi, Y.-M. Zhang, L. Xiao and Y. Liu, *J. Med. Chem.*, 2022, **65**, 13473; (b) J. Chen, H. Ni, Z. Meng, J. Wang, X. Huang, Y. Dong, C. Sun, Y. Zhang, L. Cui, J. Li, X. Jia, Q. Meng and C. Li, *Nat. Commun.*, 2019, **10**, 3546.

12 Y.-F. Ding, S. Li, L. Liang, Q. Huang, L. Yuwen, W. Yang, R. Wang and L.-H. Wang, *ACS Appl. Mater. Interfaces*, 2018, **10**, 9980.

13 (a) S. Yan, P. Sun, N. Niu, Z. Zhang, W. Xu, S. Zhao, L. Wang, D. Wang and B. Z. Tang, *ACS Nano*, 2022, **16**, 9785; (b) X. Dai, B. Zhang, W. Zhou and Y. Liu, *Biomacromolecules*, 2020, **21**, 4998; (c) W. Xu, M. M. S. Lee, J.-J. Nie, Z. Zhang, R. T. K. Kwok, J. W. Y. Lam, F.-J. Xu, D. Wang and B. Z. Tang, *Angew. Chem., Int. Ed.*, 2020, **59**, 9610.

14 S. Cui, D. Yin, Y. Chen, Y. Di, H. Chen, Y. Ma, S. Achilefu and Y. Gu, *ACS Nano*, 2013, **7**, 676.